Plasmon dispersion diagram and localization effects in a three-cavity commensurate grating

Aude Barbara, Stéphane Collin, Christophe Sauvan, Jérôme Le Perchec, Camille Maxime, Jean-Luc Pelouard, Pascal Quemerais

Plasmon dispersion diagram and localization effects in a three-cavity commensurate grating

A. Barbara,[1] S. Collin,[2] Ch. Sauvan,[2,3] J. Le Perchec,[1] C. Maxime,[1] J-L. Pelouard,[1] and P. Quémerais[1]

[1]*Institut Néel, CNRS et Université Joseph Fourier, BP 166, F-38042 Grenoble Cedex 9, France*

[2]*Laboratoire de Photonique et Nanostructures, CNRS, Route de Nozay, F-91460 Marcoussis, France*

[3]*Present address: Laboratoire Charles Fabry de l'Institut d'Optique, CNRS et Université Paris-Sud, Campus de Polytechnique, RD128, F-91127 Palaiseau, France*

aude.barbara@grenoble.cnrs.fr

Abstract: Commensurate gratings of deep-metallic grooves have highly localized cavity resonances which do not exist for purely periodic gratings. In this paper we present the experimental dispersion diagram of the resonances of a commensurate grating with three sub-wavelength cavities per period. We observe selective light localization within the cavities, transition from a localized to a delocalized mode and modifications of the coupling of modes with the external plane-wave that may lead to the generation of black modes. This unexpected complexity is analyzed via a theoretical study in full agreement with the experiments. These results open a way to the control of wavelength-dependent hot spot predicted in more complex commensurate gratings.

OCIS codes: (260.3910) Metal optics; (240.6680) Surface plasmons; (240.6695) Surface-enhanced Raman scattering; (050.6624) Sub-wavelength structures.

References and links

1. K. Kneipp, M. Moskovits and H. Kneipp, ed., *Surface-Enhanced Raman Scattering*, Topics in Applied Physics, **103,** (Springer, 2006).
2. A. Hessel and A. A. Oliner, "Wood's anomaly effects on gratings of large amplitude," Opt. Commun. **59,** 327 (1986).
3. A. Wirgin, "Resonance scattering of electromagnetic waves from a rectangular groove on a metallic mirror," Opt. Commun. **7,** 1, 70 (1973)
4. A. Wirgin and A. A. Maradudin, "Resonant response of a bare metallic grating to s-polarized light," Prog. Surf. Sci. **22,** 1 (1986)
5. A. Wirgin, T. López-Ríos, "Can surface enhanced raman scattering be caused by waveguide resonances," Opt. Commun. **48,** 416 (1984); *ibid.* "Errata", Opt. Commun. **49,** 455 (1984).
6. E. Albano, S. Daiser, G. Ertl, R. Miranda, K. Wandelt and N. Garcia, "Nature of surface-enhanced-Raman-scattering active sites on coldly condensed Ag films," Phys. Rev. Lett. **51,** 2314-2317 (1983).
7. J. Le Perchec, P. Quémerais, A. Barbara, T. López-Ríos,"Why metallic surfaces with grooves a few nanometers deep and wide may strongly absorb visible light," Phys. Rev. Lett. **100,** 066408 (2008).
8. S. Grésillon, L. Aigouy, A. Boccara, JC. Rivoal, X. Quelin, C. Desmarest and P. Gadenne, "Experimental observation of localized excitations in Random metal-dielectric films," Phys. Rev. Lett. **82,** 4520 (1999).
9. M. I. Stockman, S. V. Faleev, D. J. Bergam, "Localization versus delocalization of surface plasmons in nanosystems: can one state have both characteristics?," Phys. Rev. Lett. **87,** 167401 (2001).

#129006 - $15.00 USD Received 25 May 2010; revised 22 Jun 2010; accepted 23 Jun 2010; published 28 Jun 2010

10. A. A. Maradudin, T. Michel, A. R. McGurn and E. R. Mendez, "Enhanced backscattering of light from a random grating," Ann. Phys. (NY) **203,** 255 (1990).
11. T. A. Leskova, A. A. Maradudin, J. Munoz-Lopez, "Coherence of light scattered from a randomly rough surface," Phys. Rev. E **71,** 036606 (2005).
12. M. I. Stockman, L. N. Pandey, L. S. Muratov, T. F. George,"Giant fluctuations of local optical fields in fractal clusters," Phys. Rev. Lett. **72,** 2486 (1994).
13. E. L. Albuquerque, M. G. Cottamb, "Theory of elementary excitations in quasiperiodic structures," Phys. Reports **376,** 225 (2003).
14. T. Matsui, A. Agrawal, A. Nahata and Z. V. Vardeny, "Transmission resonances through aperiodic arrays of subwavelength apertures," Nature **446,** 517 (2007).
15. A. Barbara, J. Le Perchec, S. Collin, C. Sauvan, J-L. Pelouard, T. López-Ríos , P. Quémerais, "Generation and control of hot spots on commensurate metallic gratings," Opt. Exp. **16,** 19127 (2008).
16. C. Berger, E. Belin, D. Mayou, "Electronic properties of quasicrystals," Ann. Chim.-Sci. Mat. (Paris) **18,** 485 (1993).
17. E. Belin and D. Mayou,"Electronic properties of quasicrystals," Phys. Scr. **T49,** 356 (1993).
18. P. Quémerais, "Model of growth for long-range chemically ordered structures: application to quasicrystals," J. Phys. I France **4,** 1669 (1994).
19. F. Ducastelle and P. Quémerais, "Chemical self-organization during crystal growth," Phys. Rev. Lett. **78,** 102 (1997).
20. J. Le Perchec, P. Quémerais, A. Barbara and T. López-Ríos, "Controlling strong electromagnetic fields at sub-wavelength scales," Phys. Rev. Lett. **97,** 036405 (2006).
21. M. Navarro-Cía, D. Skigin, M. Beruete, M. Sorolla, "Experimental observation of phase resonances in metallic compound gratings with subwavelength slits in the millimiter wave regime," Appl. Phys. Lett. **94,** 091107 (2009).
22. C. Billaudeau, S. Collin, C. Sauvan, N. Bardou, F. Pardo and J-L Pelouard, "Angle-resolved transmission measurements through anisotropic 2D plasmonic crystals," Opt. Lett. **33,** 165 (2008).
23. T. López-Ríos, D. Mendoza, FJ. García-Vidal, J. Sánchez-Dehesa and B. Pannetier, "Surface shape resonances in lamellar metallic gratings," Phys. Rev. Lett. **81,** 665 (1998).
24. A. Barbara, P. Quémerais, E. Bustarret, T. López-Ríos and T. Fournier, "Electromagnetic resonances of sub-wavelength rectangular metallic gratings,"Eur. Phys. J. D. **23,** 143-154 (2003).
25. D. Skigin and R. Depine, "Transmission resonances of metallic compound gratings with subwavelength slits," Phys. Rev. lett. **95,** 217402 (2005) and references therein.
26. E. D. Palik, *Handbook of optical constants of solids*, Academic Press.
27. S. Collin, F. Pardo, R. Teissier and J.-L. Pelouard, "Strong discontinuities in the complex photonic band structure of transmission metallic gratings," Phys. Rev. B **63,** 033107 (2001).

1. Introduction

Within the vast framework of controlling light properties at a sub-wavelength scale one important issue is to understand and produce - in a reproducible manner - field localization and enhancements at the surface of metals, one reason being that those are linked to the Surface Enhanced Raman Scattering (SERS) effect[1]. Beyond the fundamental interest of understanding SERS, many applications could benefit from the possibility of controlling the local field enhancement factors. They might actually be very useful for ultra-sensitive spectroscopic techniques which are widely used for identifying molecules in physics, chemistry, biology and pharmacology.

Electromagnetic field enhancements at the surface of metals are created by the coupling of incident light with the surface plasmon modes of the metal. The resulting hybrid mode called surface plasmon-polariton (SPP) can, roughly speaking and in the context of a given surface topology, either be delocalized in which case it enables to transfer energy within the system, or be localized in which case it permits to confine electromagnetic energy within a sub-wavelength volume. The confinement may occur inside pits or crevasses, with heights $h \sim \lambda$, λ being the wavelength of the incident exciting wave, when the SPP are excited in the optical regime (short wave numbers)[2, 3, 4, 5] or inside cavities with $h \ll \lambda$ when the SPP are excited in the electrostatic regime (long wave numbers)[6, 7]. Localization of the electromagnetic field may also occur at the surface of disordered systems[8, 9, 10, 11] and is then related to the multiple scattering of the SPP by the surface roughness or by the metallic

#129006 - $15.00 USD Received 25 May 2010; revised 22 Jun 2010; accepted 23 Jun 2010; published 28 Jun 2010

nanoparticles. Lastly, another type of localization occurs in self-similar systems, such as fractal clusters[12] or quasiperiodic structures[13, 14], which can be regarded as systems with a deterministic (or controlled) disorder[13]. In a previous paper we proposed an alternative manner to induce light localization phenomena by considering commensurate gratings of deep sub-wavelength metallic grooves. By doing so, we combined the effects of light trapping within active sites (the deep cavities) with the properties of self-similar arrangements (commensurate gratings) and this in a controlled and applicable manner since the theory, the engineering of the sample and the experiments can be achieved[15]. Our results showed that, as it occurs for electron localization in quasi-crystal for instance[16, 17], new light localization phenomena arise from merging electromagnetic resonances of deep metallic grooves with one-dimensional commensurate structures.

In this paper, we present the detailed study of the electromagnetic resonances of a three-cavity per period commensurate grating. These resonances are due to the near-field coupling of the cavities within a period and consequently do not exist for a simple period grating. Dispersion diagrams of the modes are measured and analyzed for the first time, here in the infra-red region. We observe a very information-rich diagram in terms of dispersion of the different modes and in their extinction. Apart form the surface plasmons, three cavity resonances are observed. One vanishes at normal incidence and is then excited over the whole diagram. Moreover, this mode undergoes a transition from a localized to a partly delocalized state, due to its coupling with horizontal surface plasmons as the incident angle increases. In contrast, the second cavity mode does not couple with horizontal surface plasmons and remains localized. Moreover it becomes, within a range of several degrees of the incidence angle of the impinging wave, a "black-mode" in the sense that it also does not couple with the incident wave. Finally, the third cavity resonance behaves in a manner similar to that of a simple period grating. We analyze these features in the framework of the modal expansion approach [4] which is in full agreement with the experiments. All these phenomena are discussed along the paper.

2. Experiments

2.1. Commensurate gratings and experimental set-up

Before we focus on the sample studied, let us briefly recall what the commensurate gratings we are dealing with are. Commensurate gratings are long-period gratings containing several identical, deep, rectangular and sub-wavelength aperture grooves per period. Within the period, two consecutive cavities may be separated either by a long distance L or a shorter one S, their order of appearance being such that no additional periodicity arises. As we increase the number of grooves within a period, we create more and more complex periodic gratings. The period tends to infinity and the arrangement of the grooves within a period tends, in a self-similar manner, to an aperiodic sequence[18, 19]. By this approach we can study the gradual apparition and modifications of light localization effects, starting from a simple-period grating to an almost aperiodic one[15]. We have previously theoretically predicted that critically wavelength-dependent hot spots could be generated and controlled from far-field considering such arrangements. Strong and sharp electromagnetic resonances appear. They are due to new cavity resonances which do not exist for gratings with one cavity per period. These states are more or less radiative depending on the coupling between the cavities[20] and will consequently exhibit different enhancement factors and coupling with the incident exciting wave. Their localization may also be altered by coupling with horizontal surface plasmons. The far-field signatures of these modes are dips observed in the reflectivity measurements of p-polarized light. They have been recently evidenced experimentally for the first time, in the infra-red region[15] and in the microwave regime[21] for gratings with two or three slits per period.

#129006 - $15.00 USD Received 25 May 2010; revised 22 Jun 2010; accepted 23 Jun 2010; published 28 Jun 2010

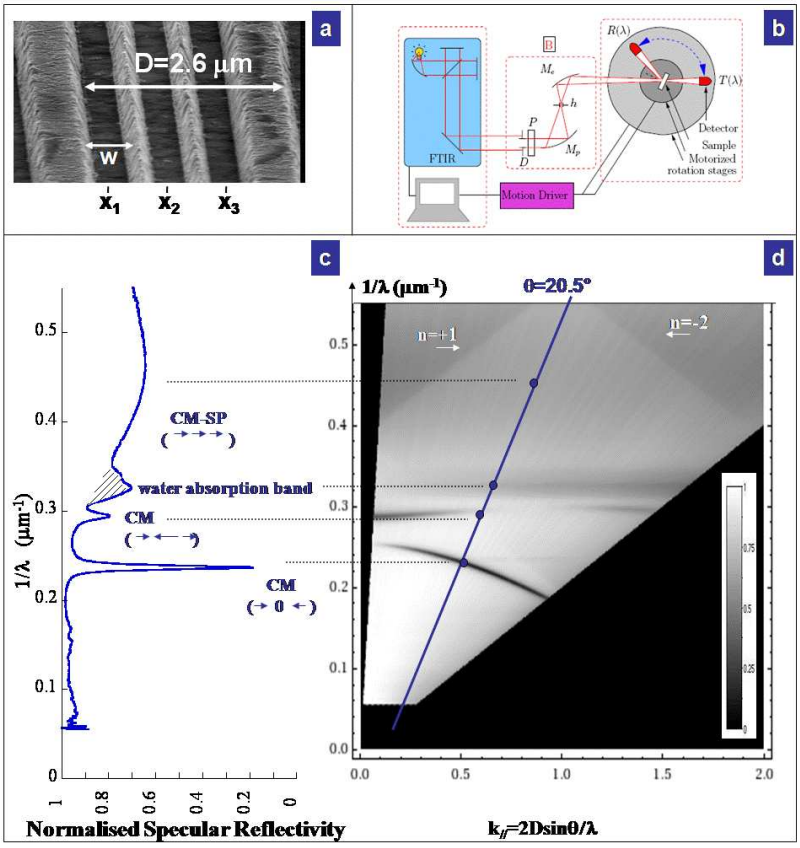

Fig. 1. (a) SEM image of the gold grating and (b) experimental set-up as described in [22]. The sample is mounted in the center of the motorized stage. For each $\theta/2\theta$ position of the sample/detector, specular reflectivity as a function of the incident wavelength is measured. (c) shows the spectrum measured at $\theta = 20.5°$ corresponding to a scan along the blue line added in the experimental dispersion maps displayed in (d). The dispersion diagram is obtained from the normalized intensity of the specular reflectivity plotted as a function of the in-plane wave vector $k_{//}$ and the wave number $1/\lambda$. The excited modes appear as dips in the specular reflectivity dips and as dark lines in the dispersion diagram. The hatched peak is due to the infra-red absorption of residual water in the experiment set-up.

In this paper we report on the measurements and analyze the dispersion of the modes of a gold commensurate grating whose unit cell is composed of three grooves positioned at x_1=0, x_2=0.7 μm and x_3=1.4 μm respectively and whose period is D=2.6 μm. These parameters were chosen in order to have resonances in the infra-red region. Figure 1a displays the SEM image of the grating which was fabricated using electron-beam lithography and a double lift-off technique described in ref.[15] and references therein. The grooves obtained are trapezoidal with a height h=0.59 μm and a width w=0.36 μm at the bottom and w=0.62 μm at the top. In the calculations we took w =0.62 μm.

The dispersion curves of the excited modes are obtained by measuring the specular reflectivity of the grating illuminated by a p-polarized light in the spectral range $1.5 - 16\mu m$ and at various incident angles θ ranging from $2.5 - 74°$ with a step of 0.5°. For each angle, the specular reflectivity measured as a function of the wave number of the incident light is nor-

#129006 - $15.00 USD Received 25 May 2010; revised 22 Jun 2010; accepted 23 Jun 2010; published 28 Jun 2010

malized by that of a flat gold surface performed in the same spectral range and at $\theta = 2.5°$. As an example, the reflectivity spectrum measured at $\theta = 20.5°$ is shown in figure 1c. The experimental set-up, whose geometry is sketched in figure 1b, is based on a commercial Fourier transform spectrometer and a home-made optical system permitting a spectral resolution of 10 cm^{-1} and a convergence angle $\Delta\theta = \pm 0.5°$[22]. The sample and the detector are mounted on two co-axial motorized stages permitting $\theta/2\theta$ reflectivity measurements. The resulting dispersion diagram (figure 1d) is a gray scale intensity map of the normalized specular reflectivity plotted as a function of the normalized in-plane wave-vector $k_{//} = (2Dsin\theta)/\lambda$ in abscissa and the wave-number $1/\lambda$ in ordinate.

2.2. Experimental results

As can be observed in figure 1c, the grating presents three cavity modes (CM) in the 0.4-0.55 μm^{-1} spectral range. In the dispersion diagram (Fig.1d) they appear as dark lines, the two darkest ones corresponding to the two narrow resonances. Two additional straight-line dispersions are also visible in the dispersion diagram. They correspond to the branches $n = +1$ and $n = -2$ of the well-known horizontal surface plasmon (SP) propagating along a metal/air interface of a periodic system as $1/\lambda = \pm n/D(\sqrt{\varepsilon/(\varepsilon+1)} \pm sin\theta)$. The branch $n = -1$, that should start at $1/\lambda$=0.385 μm^{-1} at normal incidence, is not clearly observed since it forms a coupled mode with the broad cavity mode observed at 0.45 μm^{-1}. Lastly, water condensation on the detector window gives rise to the non-dispersive water absorption bands hatched in the figure to distinguish them from the resonances of the grating.

The three cavity resonances result from the non-periodic arrangement of the cavities within the period of the grating which modifies their near-field coupling. This coupling splits the cavity resonance, of an individual cavity or of a simple-period grating[23], into three resonances[15]. The striking point of these resonances is that two of them are spectrally very narrow i.e they are only weakly radiative and they have a large quality factor Q. The third resonance has a broad bandwidth. It is more radiative and has consequently a smaller Q factor and an enhancement factor. At first sight one can notice that the two narrow cavity modes exhibit a very different behaviour: the lower wave number branch vanishes at normal incidence and disperses very strongly when the incidence angle increases. Conversely the higher wave-number mode disperses very weakly, as it is expected for a cavity mode, and is strongly excited at normal incidence. However, its excitation strength unexpectedly diminishes down to extinction in the range $k_{//}$=0.75 to 0.94 which corresponds to incident angles θ=29 to 37°. These features show that this commensurate grating with only three cavities per period already presents sophisticated localization effects that need to be thoroughly investigated.

3. Results analysis

3.1. Theoretical method

In order to understand the complexity of the dispersion diagram we have calculated the optical response of the grating following the approximated modal method developed for simple-period gratings[4, 24] and adapted it to commensurate arrangements[15]. The modal method consists in expanding fields inside the cavities on the different modes of the cavity and in expanding the fields in the free space above the grating by a Rayleigh development. For a p-polarized incident plane wave and a grating lying in the (x,z) plane, only the transverse component of the magnetic field H_z needs to be expressed[24]. Above the grating the latter is the sum of the incident beam and of all the reflected diffraction orders:

$$H_z^{(I)}(x,y) = e^{ik(\gamma_0 x - \beta_0 y)} + \sum_{m=-\infty}^{m=+\infty} R_m e^{ik(\gamma_m x + \beta_m y)}, \quad (1)$$

#129006 - $15.00 USD Received 25 May 2010; revised 22 Jun 2010; accepted 23 Jun 2010; published 28 Jun 2010

with $k = 2\pi/\lambda$ being the wave vector of the incident plane wave. The terms $\gamma_m = sin\theta + m\lambda/D$, $\beta_m^2 = 1 - \gamma_m^2$ and R_m are the normalized wave vectors and the amplitude of the m^{th} order of reflection respectively.
In the grating, the field is the sum of the field inside each cavity. The expression of the field in the p$^t h$ cavity is obtained by considering the vertical walls as perfectly conducting and the impedance condition at the bottom of the cavity. It writes as:

$$H_{z,p}^{(II)}(x,y) = \sum_{\ell=0}^{+\infty} A_{\ell,p} \cos\left[\frac{\ell\pi}{w}\left(x - x_p + \frac{w}{2}\right)\right]\left(e^{i\mu_\ell(y+2h)} + r_\ell e^{-i\mu_\ell y}\right). \quad (2)$$

where A_p^ℓ and $\mu_\ell = k\sqrt{1-(\frac{\ell\lambda}{2w})^2}$ are the amplitude and the vertical component of the wave vector of the ℓ^{th} mode in the p^{th} cavity respectively. x_p is the coordinate of the center of the p^{th} cavity. The general expression of the series of x_p of complex commensurate gratings can be found in ref.[15, 18, 19]. The coefficients $r_\ell = (\mu_\ell/k + \eta)/(\mu_\ell/k - \eta)$ are the reflection coefficients of the ℓ^{th} mode at the bottom of the cavity, where $\eta = 1/\sqrt{\varepsilon}$ and ε is the relative dielectric constant of the metal.
After applying the boundary conditions at the interface between the grating and the free space above, one obtains a matrix system of the form **M.A=V** where **A** is the vector of the amplitudes $(A_{\ell,p})$, **M** is a $(3L \times 3L)$ matrix -L being the number of modes considered inside the cavities (eq. 2)- and **V** is related to the excitation vector (incident field). A second expression, linking the reflection coefficients R_m to the amplitude vector **A** is also obtained. This relation is given in the appendix at the end of the paper together with the expressions of **M**, **A**, **V** and the procedure to obtain them. A numerical solving of the matrix system permits to determine the amplitudes $(A_{\ell,p})$ from which the R_m are calculated. The understanding of the experiments is then done as follows: the theoretical model and the geometrical parameters of the grating are validated by confrontation of the calculated specular reflectivity- $R_0 R_0^*$- with the experimental one. Localization phenomena associated to the observed resonances are determined by calculating the maps of the magnetic near-field intensities at the frequency and incidence angle corresponding to the resonance condition. The model also permits to analyze the nature of the modes. In order to do that we have determined the eigenmodes of the grating (det(**M**)=0) and the nature of their coupling to the exciting field (projection of **V** on the eigenvectors). This permits a full understanding of the origin of the resonances and of their respective width, dispersion and conditions of extinction. All these points are described hereafter.

3.2. Eigenmodes of the grating

The determination of the eigenmodes of the system, i.e the resonances supported by the grating in the absence of excitation, permits to gain an insight in the origin and the nature of the three resonances observed. An eigenmode exists each time det(**M**)=0 (or real part: $\Re$(det(**M**)=0) for a complex matrix). This condition is numerically found by diagonalizing **M** and finding the frequency and incident angle (related to the value of $k_{//}$) for which at least one eigenvalue is null.
In our case of a grating with sub-wavelength aperture grooves, we know that the resonances are essentially contented in the fundamental mode of the cavities since it is the only propagative one[24]. Considering only this first mode ($\ell = 0$ in eq. 2) reduces **M** to a (3×3) matrix presenting three eigenvalues $e_{i=1,2,3}$ associated with three eigenvectors $\mathbf{U_{i=1,2,3}}$. Since the eigenvalues are complex, the system presents an eigenmode each time that the real part of e_i (noted $\Re(e_i)$) is null, the remaining imaginary part, $\Im(e_i)$, being linked to the width of the resonance. The

#129006 - $15.00 USD Received 25 May 2010; revised 22 Jun 2010; accepted 23 Jun 2010; published 28 Jun 2010

frequency for which the annulation occurs is the resonance frequency. The eigenvectors respectively associated with the eigenvalues at the resonance frequency also permit to characterize the eigenmode since they have three complex components proportional to the amplitude (module) and to the phase (argument) of the electromagnetic field inside the three cavities respectively. A field localization distribution can thus be associated with each eigenmode. In the present case, the annulation of the eigenvalues of $\mathbf{M}$ in the 0.4-0.55 $\mu\mathrm{m}^{-1}$ does highlight the three cavity resonances observed and on which we will focus our attention. According to the experiments, the numerical analysis shows that out of the three resonances two of them have thin widths, $\Im(e_1) \simeq -0.01$ and $\Im(e_2) \simeq -0.03$, and one is large $\Im(e_3) \simeq -4.5$. These modes are associated with the eigenvectors $\mathbf{U_1} \approx (1,0,-1)$, $\mathbf{U_2} \approx (1,-2.3,1)$ and $\mathbf{U_3} \approx (1,1,1)$ respectively. Let us note that these vectors do not form an orthogonal basis.

In the case of a two-groove system illuminated by a p-polarized light, we previously showed [20] that its optical response could be understood by analogy with the scattering of a p-polarized electromagnetic wave by a system of two dipole centers separated by a sub-wavelength distance. Each resonant cavity actually localizes an electric field oriented along the horizontal x-axis and oscillating at ωt and acts as a forced oscillating dipole. The near-field coupling of the two dipoles induces the resonances observed (see details in ref.[20]). Following this analysis we may here consider three identical dipoles separated two-by-two by a distance $d << \lambda$, where $\lambda = 2\pi/k$ is the wavelength of the scattered electromagnetic wave. The optical response will be analogous to a three-groove system. Each dipole is characterized by a resonance frequency ω_0, a resonance width $\gamma_0 \approx 2w\omega_0^2/\pi c$ and an effective electromagnetic radius $r_0 \approx 2w/c$. This system presents three resonances: a spectrally broad one associated with the eigenvector $(1,1,1)$ and two spectrally narrow ones associated with the eigenvectors (1,0,-1) and $(1, \approx -2, 1)$. The resonance of the unique dipole thus splits into three resonances and the widths of these resonances are directly related to the effective electromagnetic radius r_0 of the mode, and therefore to the radiation damping. The mode corresponding to the three dipoles in-phase has an effective electromagnetic radius about three times that of the unique one r_0 and is consequently about three times larger ($r_3 \approx 3r_0$). In contrast, the two other modes are found to have a very thin spectral width due to their almost zero effective radius ($r_2 \approx r_0(kd/2)^2$ and $r_1 \approx r_0(kd)^2$) coming from the anti-symmetrical coupling of the dipoles.

The grating considered in this paper can be seen as a three-groove system periodically reproduced. Its optical response is thus quite close to that of a unique three-groove system. Consequently we may deduce that the resonances we observe in the case of the grating are the following: the first mode, associated with $\mathbf{U_1}$, is an out-of phase resonance of the two external slits, which localize the same amount of electromagnetic energy, leading to the extinction of the field inside the central cavity. This anti-symmetrical mode will be denoted $(\rightarrow 0 \leftarrow)$. The second mode, associated with $\mathbf{U_2}$ is an in-phase resonance of the two external slits, both out-of phase with respect to the central one. The latter localizes an electromagnetic energy four times larger than the one in the external slits (twice larger in amplitude). Due to the symmetrical coupling of the external cavities this mode will be called a pseudo-symmetric mode and denoted $(\rightarrow\longleftarrow\rightarrow)$. Lastly, the third mode, associated with $\mathbf{U_3}$ and denoted $(\rightarrow\rightarrow\rightarrow)$ corresponds to the in-phase resonance of the three cavities which all localize the same electromagnetic energy. The latter is a purely symmetric mode. It is equivalent to the usual Fabry-Perot-like resonance of the simple-period grating for which all the cavities also resonate in-phase. The phase-difference obtained between the cavities are in full agreement with the phase-resonance description of similar modes observed in compound gratings[25]. The widths of the resonances of the gratings are essentially driven by the radiation losses which depend on the different phases of the resonating grooves. The broad mode $\mathbf{U_3}$ has a large radiative damping and will consequently weakly localize the electromagnetic energy. By contrast, the two thin modes $\mathbf{U_1}$ and $\mathbf{U_2}$ have less radiation

#129006 - $15.00 USD Received 25 May 2010; revised 22 Jun 2010; accepted 23 Jun 2010; published 28 Jun 2010

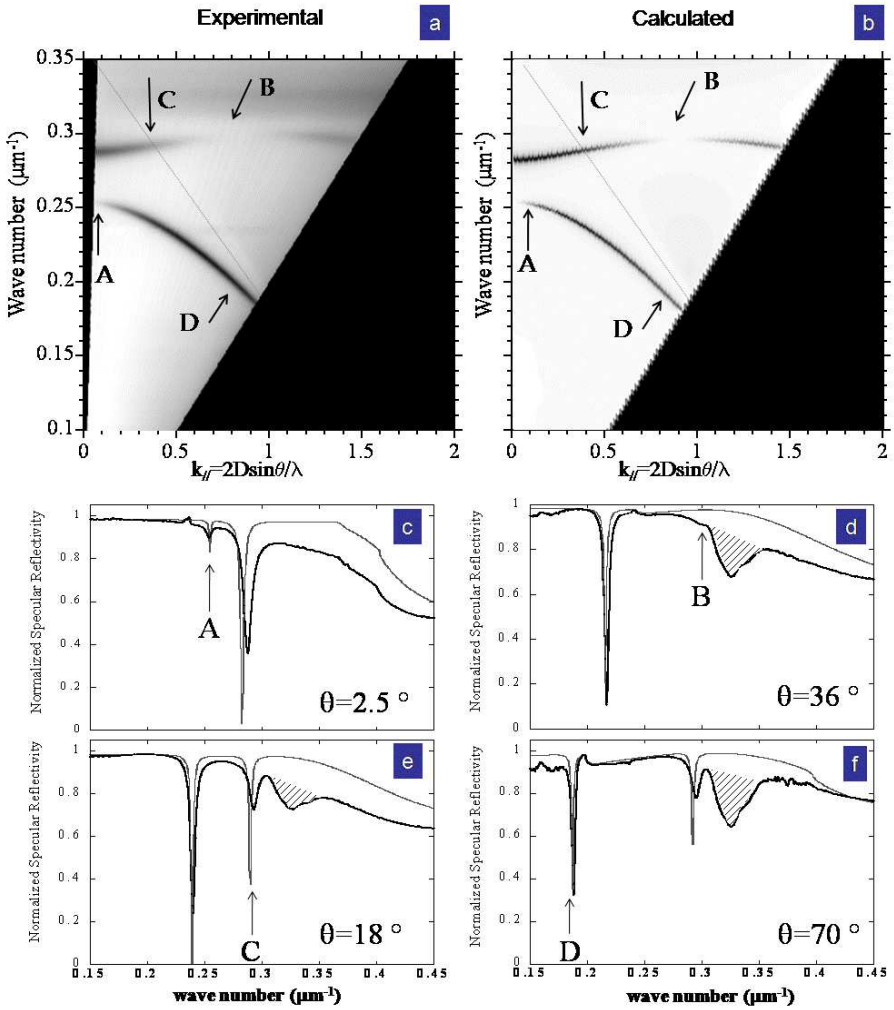

Fig. 2. Experimental (a) and calculated (b) dispersion diagram of the two thin cavity modes of the grating. The dashed line indicates the theoretical dispersion of the plasmon branch $n = -1$. (c) to (f): experimental (black) and calculated (gray) spectra measured at an incidence angle $\theta = 2.5°$ showing the weak excitation of the anti-symmetrical mode $(\rightarrow 0 \leftarrow)$ (c), $\theta = 36°$ where the pseudo-symmetrical mode $(\rightarrow\longleftarrow\rightarrow)$ is extinguished (d), $\theta = 18°$ where the pseudo-symmetrical mode should cross the horizontal surface branch (e) and $\theta = 70°$ where the anti-symmetrical mode couples with the surface plasmon branch (f). The hatched dip is due to water pollution in the experiment.

#129006 - $15.00 USD Received 25 May 2010; revised 22 Jun 2010; accepted 23 Jun 2010; published 28 Jun 2010

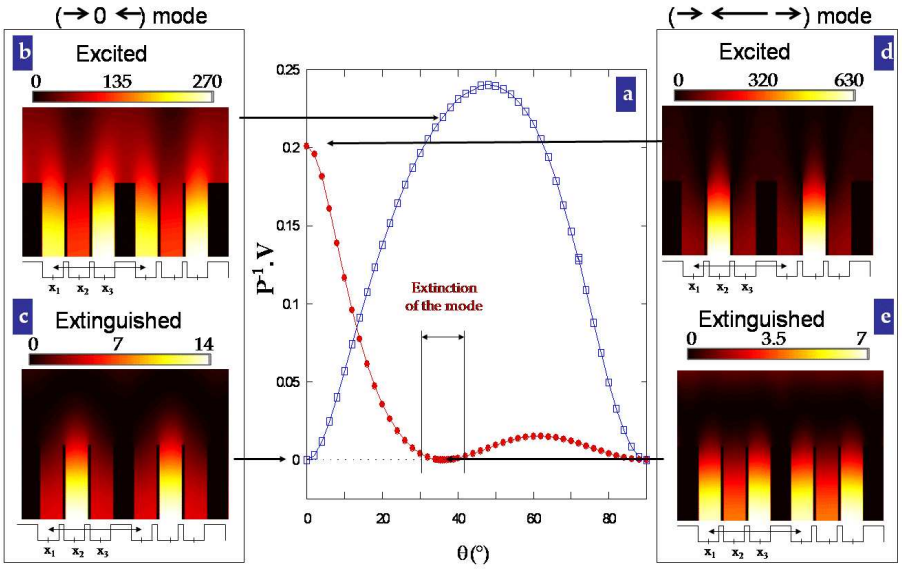

Fig. 3. (a) Projection as a function of the incidence angle of the eigenvectors $\mathbf{U_1}$ (squares) and $\mathbf{U_2}$ (dots) on the excitation vector $\mathbf{V}$. (b-e) Intensity maps of the magnetic near-field intensity for the anti-symmetrical mode calculated at $\theta = 36°$, $1/\lambda = 0.215\mu\text{m}^{-1}$ (b) and at $\theta = 0°$, $1/\lambda = 0.255\mu\text{m}^{-1}$ (c) and for the pseudo-symmetrical mode calculated at $\theta = 36°$, $1/\lambda = 0.296\mu\text{m}^{-1}$ (d) and $\theta = 0°$,$1/\lambda = 0.283\mu\text{m}^{-1}$ (e). The color bar gives the scale of the normalized magnetic field intensities.

losses and will present strong enhancement factors of the field intensities.

3.3. Excited modes: dispersion, extinction and coupling with the horizontal SP

Let us now focus on the excitation of the two thin cavity modes. The description of the broad mode $(\rightarrow\rightarrow\rightarrow)$ is similar to that of the usual cavity resonance of a simple period grating and can be found in the literature[4, 23]. Figure 2 shows a detail of the experimental dispersion diagram and that of the calculated one, together with spectra obtained at several incidence angles. Just as for the experimental diagram, the calculated one is a gray-scale map of the specular reflectivity spectra obtained by calculating the coefficients $R_0 R_0^*$ as a function of the wave-number for different angles. The gold dielectric constants were taken from ref.[26] and eight modes inside the cavities were considered (ℓ=8 in eq.2). Figures 2a and 2b show that the calculation reproduces in a very convincing manner all the features of the experiments: the positions, the dispersion, the relative intensities and the regions of extinction of the two resonances. A more quantitative comparison also gives a very good agreement between experiments and calculations as can be seen on the spectra presented on figure 2c-2f. Beyond this quantitative comparison, these four spectra were chosen because they contain specific points of the dispersion diagram (points A to D on figure 2a). They were respectively measured and calculated at the following incidence angles: θ= 2.5° showing the quasi-extinction of the anti-symmetrical mode (point A); θ=36° showing the extinction of the pseudo-symmetrical mode (point B); θ=70° showing the anti-symmetrical coupled with the $n = -1$ SP branch (point D) and θ=18° showing the crossing point between the $n = -1$ SP branch and the pseudo-symmetrical mode (point C).

The disappearance of the anti-symmetrical mode at normal incidence was previously reported for analogous systems[25, 20] and can be easily understood in terms of geometric arguments:

#129006 - $15.00 USD Received 25 May 2010; revised 22 Jun 2010; accepted 23 Jun 2010; published 28 Jun 2010

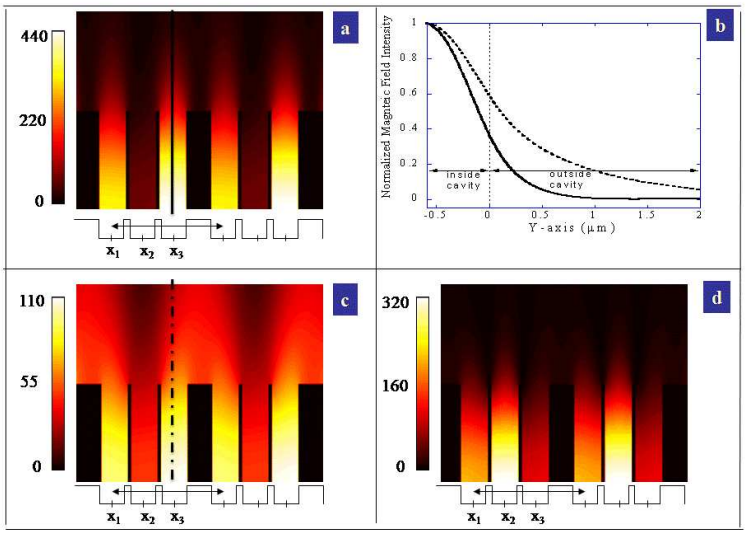

Fig. 4. Intensity maps of the magnetic field of the anti-symmetrical mode when excited at $\theta = 10°$, $1/\lambda = 0.249\mu\text{m}^{-1}$ (a) and at $\theta = 66°$, $1/\lambda = 0.188\mu\text{m}^{-1}$ (c). (b) shows the magnetic field intensity along the solid black line in (a) and the dotted line in (b). At $\theta = 10°$ the mode $(\rightarrow 0 \leftarrow)$ is strongly confined inside the cavities. Its expansion outside the cavities increases at larger incident angles due to its coupling with the horizontal surface plasmon. (d) Intensity maps of the magnetic field of the pseudo-symmetrical mode $(\rightarrow\leftarrow\rightarrow)$ when excited at $\theta = 18°$, $1/\lambda = 0.29\mu\text{m}^{-1}$.

at such incidence the exciting incident field is constant on the surface (i.e. completely symmetrical) and cannot couple to the anti-symmetrical mode. This point can also be deduced numerically by expressing the excitation vector $\mathbf{V}$ on the basis of the eigenvectors. This is done by calculating the product $\mathbf{P^{-1}}.\mathbf{V}$ where $\mathbf{P^{-1}}$ is the inverse matrix of the matrix $\mathbf{P}$ whose columns are the eigenvectors and which diagonalizes $\mathbf{M}$. The column vector $\mathbf{P^{-1}}.\mathbf{V}$ has three components equal to the projection of $\mathbf{V}$ on the three eigenvectors $\mathbf{U_{i=1,2,3}}$ respectively. Each projection is thus proportional to the coupling with the mode to the external field; when it is null the mode is a "black" mode in the sense that it cannot be excited by the external field. Figure 3a displays the projection of $\mathbf{V}$ on the eigenvectors $\mathbf{U_1}$ as a function of the incidence angle. It confirms that the coupling with the mode to the external field is null at normal incidence and that it progressively increases with the angle. The same numerical approach has been done to understand the extinction of the pseudo-symmetrical mode $(\rightarrow\leftarrow\rightarrow)$ which is much less intuitive than the previous one. The projection of $\mathbf{V}$ on the eigenvector $\mathbf{U_2}$ (fig. 3a) demonstrates that the component of $\mathbf{V}$ along this mode is maximum at normal incidence and that it diminishes when increasing the incident angle. This product, and therefore the coupling of this mode with the external incident field vanishes in a range of angles θ ~32-40°, which is in full agreement with the experimental extinction of the mode observed.

All these results are supported by the intensity maps of the magnetic field in the near-field of the grating shown in figure 3b-e. At the angles of efficient coupling of the modes with the external field, i.e at θ=36° for the anti-symmetrical mode $(\rightarrow 0 \leftarrow)$ and at normal incidence for the pseudo-symmetrical mode $(\rightarrow\leftarrow\rightarrow)$, the maps present strong enhancement factors indicating the large amount of electromagnetic energy localized inside the cavities. This localization is cavity-selective according to the distributions imposed by the symmetry of the modes: the anti-symmetrical mode associated with an eigenvector of the form (1,0-1) localizes

#129006 - $15.00 USD Received 25 May 2010; revised 22 Jun 2010; accepted 23 Jun 2010; published 28 Jun 2010

a large amount of electromagnetic intensity in the two external cavities while the central one is almost extinguished (fig. 3b) and the pseudo-symmetrical mode whose eigenvector takes the form $(1, \approx -2, 1)$ localizes an electromagnetic field intensity in the central cavity about four times larger than the two external cavities (Fig. 3d).
When considering the maps calculated at the respective extinction angles of the modes, i.e at θ=0° for the anti-symmetrical mode $(\rightarrow 0 \leftarrow)$ and at θ=36° for the pseudo-symmetrical mode $(\rightarrow\longleftarrow\rightarrow)$, the maps hardly show any enhancement factor of the fields. Only a weak near-field subsists inside the cavities and its distribution is interestingly not that of the resonant mode but that of the non-resonant mode. The distribution of the pseudo-symmetrical mode (resp. anti-symmetrical mode) appears at the resonant frequency and angle of the extinction of the anti-symmetrical mode (resp. pseudo-symmetrical) as shown in figure 3c (resp. 3e). The resonant mode is thus fully extinguished and the non-resonant one is very weakly excited due to the spectral expansion of the modes which permits a slight overlap.
Let us now comment on the dispersion of the modes and their coupling with the horizontal surface plasmons. A cavity mode is expected to very weakly disperse since it is a localized mode whose resonance frequency is mainly driven by the height of the cavity[23]. This is what we observe for the pseudo-symmetrical mode. However, the anti-symmetrical mode disperses very strongly. To understand this point we recall that the grating has a period $D = 2.6\mu m$ and should consequently support an horizontal surface plasmon in this spectral range, at a position highlighted in figure 2 by the added gray dotted line. In simple-period gratings, when a SP branch crosses a cavity mode branch, an energy splitting occurs: two hybrid modes separated by an energy gap centered on the crossing point appear[24, 27]. Here each mode has a very different behaviour. On the one hand, the pseudo-symmetrical one has no coupling with the surface plasmon branch and takes over the surface plasmon which completely vanishes. This can be seen on the map displayed in figure 4d which shows that the near-field distribution is of the type of the $(\rightarrow\longleftarrow\rightarrow)$ resonance since the enhancement of the fields is mainly localized in the central groove and since no enhancement is observed at the horizontal interface. On the other hand the anti-symmetrical mode $(\rightarrow 0 \leftarrow))$ couples with the surface plasmon and forms a unique mode. Consequently the cavity mode disperses in a manner similar to that of the surface plasmon and the mode presents a transition from a very localized state, when excited at small incidence angles, to a partly delocalized state, when excited at higher incidence angles. These features are described in figure 4: the map of the magnetic field intensity calculated considering an incidence angle $\theta = 10°$ and at the frequency resonance of the anti-symmetrical mode (fig.4a) clearly evidences the signature of the $(\rightarrow 0 \leftarrow))$ mode since a strong enhancement of the fields occurs in the two external cavities while the central one is almost extinguished. The coupling of this mode with the surface plasmon of the horizontal interface appears in figure 4c, calculated for an incidence angle $\theta = 66°$. In that case, the field is localized inside the external cavities (1 and and 3) but also above the cavities. Lastly, figure 4b shows the magnetic field intensity along the vertical direction in the middle of the third cavity. This highlights the variation of localization of the mode through its extension in the free space above the grating. A simple variation of the incidence angle can thus drive a transition from a localized to a partially delocalized state.

4. Conclusion

We have presented the first experimental dispersion diagram and the calculated one of the cavities modes appearing in a grating with more three grooves per period. The calculations reproduced in a very convincing way the unexpected features of the experimental diagram and allowed us to analyze them. In particular we have identified the nature of each resonance and studied how their coupling with the external field changes. This permitted to understand that,

#129006 - $15.00 USD Received 25 May 2010; revised 22 Jun 2010; accepted 23 Jun 2010; published 28 Jun 2010

unlike the cavity mode of a simple-period grating, the cavity resonances of our grating with three cavities per period may become black modes under particular conditions of excitation. In that case, they become non radiative and should be excited using an evanescent field. We have also shown that the coupling of the cavity modes with the horizontal surface plasmon branch $n=-1$ differs from what is observed for a simple period grating and from one mode to another. The latter is also different depending on the symmetry of the mode and can lead to partially delocalize the cavity resonance. Investigation of the coupling of higher order surface plasmon branches with cavity modes of gratings containing more than three grooves per period, and having a more complicated symmetry, would certainly lead to a better understanding of the electromagnetic localization and of the link between localized and delocalized fields.

Appendix

The following approach is based on the one described in ref.[24] for simple-period gratings and initially developed by A. Wirgin and A. Maradudin for s-polarized light[5]. The difference when dealing with commensurate gratings is that Q cavities per period need to be considered. The matrix system to be solved is obtained, in the modal approach, by applying the boundary conditions at the interface $y=0$. In the case of a p-polarized light the two conditions are:

- $\dfrac{\partial H_z^{(I)}(x,0^+)}{\partial y}+ik\eta H_z^{(I)}(x,0^+)=\dfrac{\partial H_z^{(II)}(x,0^-)}{\partial y}+ik\eta H_z^{(II)}(x,0^-)$
- $H_z^{(I)}(x,0^+)=H_z^{(II)}(x,0^-)$.

The first equality is valid over the whole interface and is projected onto the set of basis vectors $e^{(-ik\gamma_m x)}$ which leads to the following expression:

$$R_m=\frac{\beta_0-\eta}{\beta_0+\eta}\delta_{m,0}+\frac{w}{D}\sum_{p=1}^{Q}\sum_{\ell=0}^{+\infty}A_\ell^p S_{m\ell}^- e^{-ik\gamma_m x_p}\left(e^{2i\mu_\ell h}-1\right)\left(\frac{\mu_\ell/k+\eta}{\beta_m+\eta}\right), \tag{3}$$

with

$$S_{m\ell}^{\pm}=\frac{1}{w}\int_{-w/2}^{+w/2}e^{\pm ik\gamma_m x}\cos\left[\frac{\ell\pi}{w}\left(x+\frac{w}{2}\right)\right]dx.$$

The second boundary condition is valid at the mouth of each groove i.e for $x\in[x_p-w/2,x_p+w/2]$ and $p=1,2..Q$ for Q cavities per period. It is projected onto the set of basis vectors $cos\left[\frac{\ell\pi}{w}\left(x-x_p+\frac{w}{2}\right)\right]$ to obtain:

$$A_{\ell,p}=\left(\frac{2}{1+\delta_{\ell,0}}\right)\frac{1}{e^{2i\mu_\ell h}+r_\ell}\sum_{m=-\infty}^{+\infty}S_{m\ell}^{+}e^{ik\gamma_m x_p}\left(\delta_{m,0}+R_m\right). \tag{4}$$

Replacing the expression of the R_m (equation (3)) in equation (4) leads to the matrix system of the form:

$$\sum_{p'=1}^{Q}\sum_{\ell'=0}^{+\infty}M_{\ell,\ell',p,p'}A_{\ell',p'}=V_{\ell,p}$$

with

$$\begin{aligned}M_{\ell,\ell',p,p'} &= (e^{2i\mu_\ell h}+r_\ell)\delta_{\ell,\ell'}\delta_{p,p'}-F_{\ell,\ell'}\sum_{m=-\infty}^{+\infty}\frac{S_{m\ell}^{+}S_{m\ell'}^{-}}{\beta_m+\eta}e^{ik\gamma_m(x_p-x_{p'})}\\ &\text{and}\\ F_{\ell,\ell'} &= \left(\frac{2}{1+\delta_{\ell,0}}\right)\frac{w}{D}(e^{2i\mu_{\ell'}h}-1)\left(\frac{\mu_{\ell'}}{k}+\eta\right).\end{aligned}$$

#129006 - $15.00 USD Received 25 May 2010; revised 22 Jun 2010; accepted 23 Jun 2010; published 28 Jun 2010

and with

$$V_{\ell,p} = \left(\frac{2}{1+\delta_{\ell,0}}\right)\frac{2\beta_0}{\beta_0+\eta} S_{0\ell}^{+} e^{ik\gamma_0 x_p}. \tag{5}$$

The terms of the matrix **M** and that of **V** may be numerically calculated by truncation of the sums. In the unimodal approach we take $\ell = \ell' = 0$ while typically $m_{max} = 200$ reflecting orders are considered. This permits to determine the values of the coefficients $A_{\ell,p}$. From the latter, the coefficients R_m may be obtained and the electromagnetic field can be reconstructed in the whole space.

Lastly let us make a comment on the validity of the approximated modal method in the case studied here, i.e considering a gold grating studied in the infrared spectral range. In this method we consider the vertical walls of the cavities as perfect reflectors and by doing so we loose the Joule effect and the associated absorption of the energy along the walls. This effect essentially depends on the ratio of the surface impedance Z of the materials to the one of Air. Moreover, this ratio depends on the wavelength. In our case of Gold in the infrared region-at about 3000 cm^{-1} ($\lambda \sim 3.3\ \mu$m)- the ratio $Z_{Gold}/Z_{Air} \sim 0.06$, which is very small (and therefore the Joule effect too). The approximated modal method can therefore be used with confidence since it misses very few of the physics and it gives very good quantitative results both for the position of the resonances and the for the near-field in the case presented here.

#129006 - $15.00 USD Received 25 May 2010; revised 22 Jun 2010; accepted 23 Jun 2010; published 28 Jun 2010